REGISTERING SURGICAL TOOL TO A SOFT BODY USING MECHANICAL PALPATION

A TECHNICAL REPORT PREPARED FOR

NRI ANNUAL PROGRESS REPORT

YEAR 2014–2015

Rangaprasad Arun Srivatsan[1], Rajarshi Roy[2],
Long Wang[2], Nabil Simaan[2] and Howie Choset[1]

CMU-RI-TR-15-13

[1] *Carnegie Mellon University*
[2]*Vanderbilt University*

JUNE 9, 2015

Abstract

Registering a surgical tool to an a *priori* model of the environment is an important first step in computer-aided robotic surgery. Registration of the surgical tool to a flexible environment such as an organ is difficult due to organ shifting and deformation. Palpating an organ reveals stiffness information that can serve as anatomic fiducials and facilitate the registration. In this work, locally stiff features such as arteries and tumors are used to preregister the tool to the organ model. Following that, we use a Kalman filtering framework to register the surgical tool to the surface of the organ. The tissue is palpated with regulated forces and a palpation depth dependent stiffness model is used to capture the interaction between the tool and the tissue. We believe this is the first presentation of a method to preregister and register a surgical tool to a flexible environment using only mechanical palpation. The algorithm is experimentally evaluated using a 3-DOF Cartesian slave robot that interacts with a phantom tissue model. The effectiveness of the preregistration step and the registration algorithm are validated and the results demonstrate that the proposed method improves registration accuracy and the pre-registration step leads to faster convergence.

Contents

List of Figures

1 INTRODUCTION

Minimally invasive surgery (MIS) has the potential to reduce patient trauma and complications, while at the same time lowering costs and hospital stays. The reason for these benefits stems from the fact that MIS is typically performed through small incisions, as opposed to a large incision common in open surgery. While it has the aforementioned benefits, MIS is still limited by the narrow field of view, small workspace and reduced sensory information. The physician can hardly see the internal anatomy, let alone feel it. This makes it difficult for the physician to assess the current situation of a procedure, let alone correlate preoperative models, like CT scans, with the current intraoperative scene.

Integration of robotic surgery with computer-aided surgery (CAS) can assist the surgeon in overcoming some of these shortcomings of MIS. New mechanisms, such as surgical snake robots [19, 4], can increase the accessible workspace from a single incision or even a natural orifice [7]. CAS can further assist the physician in execution of the surgical task by displaying the functional and geometric information, obtained preoperatively, over the surgeon's field of view, or on a three-dimensional display, or even super-imposed over live data collected during the procedure.

The success of the CAS is contingent upon accurate registration of the surgical tool to the coordinate frame of the 3D preoperative model of the anatomy. When the anatomy is rigid, registration is relatively simple and a number of techniques have been developed to do the same [3, 2, 10, 1]. However, when dealing with tissues or soft organs, the anatomy's shape might change during the procedure due to gravitational forces or organ swelling and might complicate the task of registration. An inaccurate registration can degrade surgical execution accuracy. Already, prior work has been developed to overcome some of these challenges using geometry and imaging based techniques [20, 15]. Such methods perform poorly when obfuscated with blood or other body fluids and also respond adversely to change in lighting. In addition vision-based methods are not effective in finding critical features that might be hidden beneath layers of tissue. Ultrasound imaging and mechanical palpation can reveal such hidden features, by detecting change in local stiffness. While there has been some work on using ultrasound imaging to register rigid bodies, not much work has been done to register soft bodies.

Instead of registering the preoperative model to the visible anatomy using intraoperative imaging and sensing, this paper describes a novel registration technique using mechanical palpation. While there are approaches in literature to perform mechanical palpation to find tissue stiffness [17, 13, 23, 5, 24], we are interested in using the stiffness properties to perform registration. This work

done using a filtering approach while assuming that the tool-tissue interactions are approximated by a linear spring-based stiffness model. In this work, we relax the assumptions of linearity in the tool-tissue interactions to account for palpation depth-dependent changes in the stiffness, a commonly observed phenomena in deformable materials such as soft tissue [11]. We also utilize the experimental system presented in our previous work in [8], where an approach for stiffness and impedance exploration and autonomous motion in a deep cleft were investigated.

Furthermore, in our previous work in [16], we used the iterated extended Kalman filter (IEKF) for estimating the registration and stiffness parameters, where was initialized using an uniformative prior distribution. In this work, a pre-registration step is presented to estimate a prior for the filter which uses stiffness features segmented from a ground truth stiffness map, that can be generated either by ultrasound elastography or mechanical palpation. The pre-registration gives a good initial guess that helps in faster convergence of the filter as opposed to an uninformative prior. In addition, an unscented Kalman filtering approach is adopted with the hope of handling non linearities in process and observation model better than extended Kalman filters or iterated extended Kalman filters.

2 PROBLEM STATEMENT AND ASSUMPTIONS

Given an a-priori model of a soft body, the surgical tool needs to be registered to the frame of the model given the measurements of the tool tip positions and associated contact forces. The following are some of the assumptions that we make in this work, and their justifications:

- The position of tip of the robot used for palpation can be measured accurately either by using the kinematics of the robot or using a position sensor.
- The robot has force sensing capability, so that it can be servoed in a hybrid position-force control manner, wherein position control can be commanded in certain directions and force control can be commanded in orthogonal directions.
- The forces applied by the robot are not very high in magnitude in order to prevent large deformation and possible damage to the soft body being palpated.
- The friction between the tool tip and the surface of the soft body is negligible as the surface of the anatomy is typically lubricated and the tool tip can be made spherical and smooth.

- Individual nonlinearities in the tool-environment interactions arising out of geometric nonlinearities (due to probe geometry) and material nonlinearities (due to hyperelasticity, viscoelasticity in the organ) are lumped together in the acquisition of palpation depth dependent stiffness maps.

In this work, we first estimate the stiffness of the soft body by performing a number of controlled palpation experiments in a structured manner as described in Section 4. When doing this, we assume perfect registration between the robot tool tip and the model of the anatomy. Once we obtain the ground truth stiffness map of the anatomy, the anatomy could be displaced and positioned in any desired manner and using the framework described in this work, the tool can be registered to the frame of the model of the anatomy.

3 METHODOLOGY

In this work, we first develop a structured framework to estimate the material properties of the soft body being probed. To do this, we discretize the surface of the soft body into a grid mesh and at each of the grid points, we fit a polynomial to describe the variation of the stiffness with respect to change in palpation depth. It is worth noting that while this ground truth variation of stiffness with respect to palpation depth is calculated, perfect registration between the soft body and its CAD model is assumed. A detailed description of this is provided in Section 3.1. For any unknown position of the organ with respect to the robot base, a pre registration is performed to find a good initial registration estimate. This is done by scanning the surface at two different controlled force levels and estimating a rough stiffness contour map. Following that, the stiff regions are segmented from the contour stiffness map and the centroids of the stiff features are compared against the centroids of stiff features on the ground truth stiffness map. The registration between the centroid points of the stiff features is obtained using standard registration algorithms such as ICP [3]. Section 3.2 describes the pre registration procedure in detail. The registration is carried out by using an unscented Kalman filtering framework. The registration estimate from the pre registration step is used as the prior and the using the polynomial description for stiffness variation at grid points, the palpation force is modelled given the depth estimate at the point of palpation. The innovation step of the filter comprises of minimizing the difference between the modelled force and the measured force of palpation. Incorporating the raster palpation trajectory in the process model helps converge faster. The filtering is performed in the space of the Lie

3.1 Generating the ground truth stiffness map

In our previous work [16], we assumed a linear stiffness model for the palpated object where the stiffness did not vary with the palpation depth. In most practical applications however, this assumption is unlikely to hold due to the nonlinear material properties of biological tissues, which has been well established [6]. Capturing nonlinear material properties become crucially important when palpation is being carried out for a subsurface embedded object such as a tumor or an artery, which are located significantly below the organ surface, quite possibly beyond the linear approximation of the stiffness relating force with the palpation depth.

In order to characterize depth dependent stiffness in the palpated object, we perform the following steps (see Fig.1):

1. The surface is raster scanned with the 3 DOF cartesian robot (See Section IV for further details). The point cloud of the robot tip $\boldsymbol{p_i} = (x_i, y_i, z_i)$, the contact force $\boldsymbol{f_i}$ and the local surface normal $\boldsymbol{n_i}$ at each point $\boldsymbol{p_i}$ are acquired. The point cloud $\boldsymbol{p_i}$ and the contact force $\boldsymbol{f_i}$ are obtained in the robot base frame and the force sensor frame respectively. This process is repeated for $i = 1 \dots q$, where q is the total number of constant force scans.

2. The raw data $\boldsymbol{f}_i$, $\boldsymbol{n}_i$, and the z-coordinate of the point cloud z are fitted to a surface at prespecified X-Y planar grid points (g_x, g_y) using a linear interpolation scheme. This leads to the following fitted data $\hat{\boldsymbol{n}}_i$, $\hat{\boldsymbol{f}}_i$ and $\hat{\boldsymbol{p}}_i = (g_x, g_y, \hat{z}_i)$.

3. At each grid location (g_x, g_y), the stiffness along the local surface normal is computed using a backward difference scheme, and is given as:

$$s_i(g_x, g_y) = -\frac{\hat{\boldsymbol{n}}_{\boldsymbol{i-1}}{}^T(\hat{\boldsymbol{f}}_i - \hat{\boldsymbol{f}}_{i-1})}{\hat{\boldsymbol{n}}_{\boldsymbol{i-1}}{}^T(\hat{\boldsymbol{p}}_i - \hat{\boldsymbol{p}}_{i-1})} \tag{1}$$

   The negative sign in the right hand side of Eqn. 1 accounts for the fact that the force acting on the palpated object is opposite to the reaction force on the force sensor measuring $\boldsymbol{f}_i$. Representative stiffness maps are shown in Fig. 2.

4. At each grid location (g_x, g_y), the palpation depth d_i, computed relative to the first scan corresponding to $i = 1$, and is given by:

$$d_i = \hat{\boldsymbol{n}}_1^T(\hat{\boldsymbol{p}}_i - \hat{\boldsymbol{p}}_1) \tag{2}$$

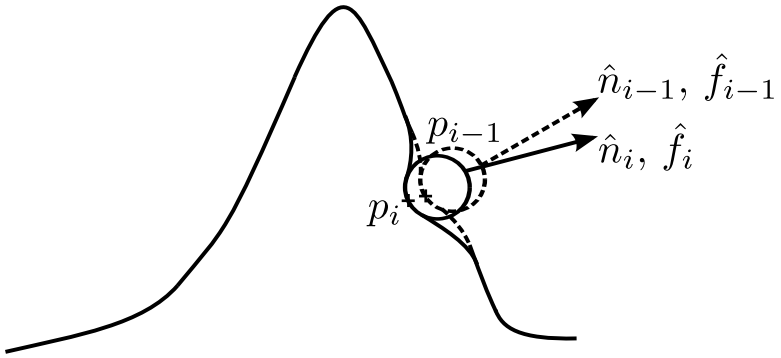

Figure 1: Schematic describing location of palpating points and the local surface normal at consecutive force scans.

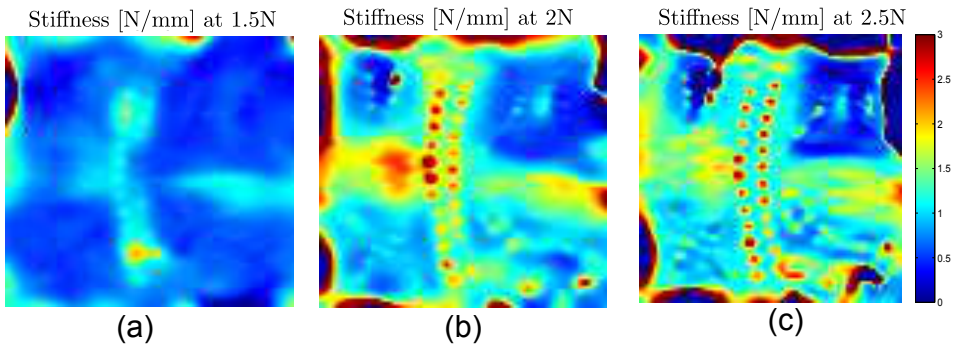

Figure 2: Representative stiffness distributions obtained at (a) $f_2 = 1.5N$, (b) $f_3 = 2.0N$ and (c) $f_4 = 2.5N$.

3.2 Pre-registration

The pre registration step is carried out to find a rough initial guess for the registration, which can then be used as a prior in the filtering process described in Section 3.3 for estimating the registration. In prior work [16], no pre-registration was done and the initial guess was arbitrarily chosen. However it will be shown in Section 5 that choosing a reasonable initial guess from a pre registration step provides more accurate registration estimate. To perform pre-registration, the organ is palpated at a very low force value. A low force value $\boldsymbol{f}_1$ would deform the surface very little and the tip positions obtained would closely emulate the points on the surface of the organ model. Following this, the organ is palpated at a higher force value $\boldsymbol{f}_2$ and the tip positions are recorded. The depth of palpation is estimated from the two palpation experiments performed and the stiffness is estimated assuming a linear stiffness model. We justify such an assumption by acknowledging the fact that in the pre registration step we are not interested in computing the exact stiffness, but instead we wish to identify the approximate locations of relatively stiff regions.

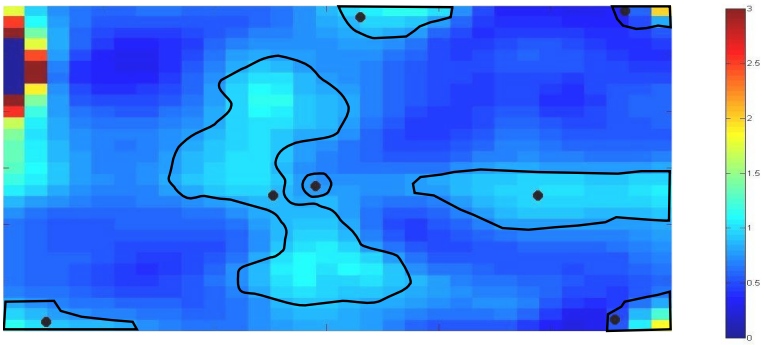

(a) Stiffness map obtained by palpating at arbitrary locations with 1.5N force. Centroids of locally stiff regions are shown by circular markers.

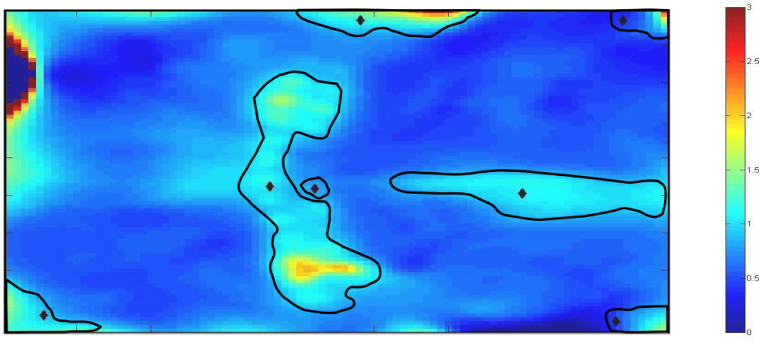

(b) Ground truth stiffness map for 1.5N force. Centroids of locally stiff regions are shown by diamond shaped markers.

Figure 3: Locally stiff regions are segmented from the stiffness map and centroid of the segmented regions are computed.

the stiff regions still appear to be at the same relative position. Thus we compare the location of the centroids of the stiff regions to infer the transformation. The regions corresponding to higher stiffness are segmented as shown in Fig. 3. Further the centroids of the segmented regions are computed. The coordinates of the centroids computed in the image frame can be readily transformed to coordinates in the frame of the robot base. Similarly the centroids of stiff regions are obtained from the ground truth stiffness map described in Section 3.1 corresponding to force $\boldsymbol{f}_2$. The coordinates of the centroids in the ground truth stiffness map can be readily transformed to the frame of the organ model. The registration between these two sets of centroids can be obtained using any standard registration technique such as ICP [3].

3.3 Registration

Registration process involves estimating the homogeneous transformation matrix $\boldsymbol{T} \in SE(3)$, that relates the reference frame fixed to the base of the robot to the reference frame attached to the model of the organ of interest. In this work, a filtering approach is followed for estimating the registration. Unlike our earlier work [21, 16] where the state vector of the filter contains Euler angles and Cartesian coordinates that parameterize $\boldsymbol{T}$, in this work the registration is carried out directly in the space of the Lie group by using a state matrix: $\boldsymbol{T}$. The underlying Lie algebra of the space is used to derive the equations of the filter as shown in [9]. Filtering in the tangent space of the group provides more accurate estimation of the state as shown in [12, 9, 14], especially in the presence of high uncertainties in the process or measurement models. In this work, we therefore adapt this approach of filtering in the space of the Lie group, instead of chooseing a Euclidean parameter space.

The state matrix is defined as:

$$\boldsymbol{X}_k = \boldsymbol{T}, \quad \text{where } \boldsymbol{T} = \begin{pmatrix} \boldsymbol{R} & \boldsymbol{t} \\ \boldsymbol{0} & 1 \end{pmatrix}, \tag{4}$$

where $\boldsymbol{R} \in SO(3)$ is the rotation matrix and $\boldsymbol{t} \in \mathbb{R}^3$ is the translation vector. We use a UKF in this work as it is known to handle non-linearities in the process and measurement models better [22]. The unscented filtering framework involves computing intermediate states called 'sigma points' which are propagated through the non-linear process and measurement models of the system.

3.3.1 Sigma point computation

calculated in the Euclidean tangent space:

$$\boldsymbol{\sigma}^0 = \boldsymbol{x}, \tag{5}$$

$$\boldsymbol{\sigma}^m = \boldsymbol{x} + \left(\sqrt{(M+\lambda)P}\right)_m, \quad m = 1, \ldots, M \tag{6}$$

$$\boldsymbol{\sigma}^m = \boldsymbol{x} - \left(\sqrt{(M+\lambda)P}\right)_m, \quad m = M+1, \ldots, 2M \tag{7}$$

where $M = 6$ the dimension of the tangent space of $SE(3)$, $\hat{\boldsymbol{x}} = \log \boldsymbol{X}$ are the exponential coordinates that describe $\boldsymbol{X}$, $(\sqrt{\cdot})_m$ denotes m^{th} column of the Cholesky decomposition and λ is a parameter for controlling the distance between the sigma points and the mean. The sigma points obtained are then projected to the manifold describing $SE(3)$ using the matrix exponential: $\boldsymbol{\sigma}^m_{SE(3)} = \exp \boldsymbol{\sigma^m}$, where $m = 0, \ldots, 12$.

3.3.2 Process and measurement models

The filtering process comprises of two main steps: prediction and update. In the prediction step, a process model is used to predict the future state of the system given it current estimate and in the update step, sensor data is used to correct the state estimate. In this work, the process model is designed to be static i.e., $\boldsymbol{X}_{k|k-1} = \boldsymbol{X}_{k-1|k-1}$ and $\boldsymbol{P}_{k|k-1} = \boldsymbol{P}_{k-1|k-1}$. The control input for the system is the estimated tip position of the robot. The tip position is estimated using another UKF as described in Section 3.3.4. The controlled force applied to the organ during the palpation serves as the measurement. The measurement model for this system is:

$$h(\boldsymbol{X}_k) = \delta_k S(\boldsymbol{p}_c, \delta_k), \quad \text{where } \delta_k = \boldsymbol{n}^T(\boldsymbol{p}_c - \boldsymbol{p}_c^{tip}), \tag{8}$$

where the subscript c denotes quantities in the frame of the organ model and $S(\boldsymbol{p}_c, \delta_k)$ is a function that returns the stiffness value associated with a point $\boldsymbol{p}_c$ on the organ model when palpated to a depth δ_k, as described in Section 3.1. The point $\boldsymbol{p}_c^{tip} = \boldsymbol{R}_k \boldsymbol{p}_r^{tip} + \boldsymbol{t}_k$, where $\boldsymbol{X}_k = \begin{pmatrix} \boldsymbol{R}_k & \boldsymbol{t_k} \\ \boldsymbol{0} & 1 \end{pmatrix}$ and $\boldsymbol{p}_r^{tip}$ is in the frame of the robot base as estimated is Section 3.3.4. In Eq. 8, the surface normal $\boldsymbol{n}$ is obtained by finding the normal associated with the point $\boldsymbol{p}_c$ on the organ model. The measurement function Eq. 8 is evaluated at the sigma points obtained earlier:

$$y_k = \sum_{m=0}^{12} w_m h(\boldsymbol{\sigma}_{SE(3)}), \tag{9}$$

where the weights w_i are defined as:

3.3.3 Update step

The update step uses the sensor data z_k to update the mean and variance and obtain $\boldsymbol{X}_{k|k}$ and $\boldsymbol{P}_{k|k}$. The covariance and cross-covariance required to compute the Kalman gain are:

$$\boldsymbol{P}_{yy} = \sum_{m=0}^{1} 2w_m(h(\boldsymbol{\sigma}^m_{SE(3)}) - y_k)(h(\boldsymbol{\sigma}^m_{SE(3)}) - y_k)^T,$$
$$\boldsymbol{P}_{xy} = \sum_{m=0}^{1} 2w_m(\boldsymbol{\sigma}^m - \boldsymbol{x}_{k|k-1})(h(\boldsymbol{\sigma}^m_{SE(3)}) - y_k)^T.$$

The Kalman gain can be obtained as $\boldsymbol{K} = \boldsymbol{P}_{xy}\boldsymbol{P}^{-1}_{yy}$. The sensor measures the normal force applied to the organ and thus we have $z_k = F_{\boldsymbol{n}}$. The estimate of the state is updated as follows:

$$\boldsymbol{X}_{k|k} = exp(\boldsymbol{x}_{k|k-1} + \hat{\boldsymbol{K}}(z_k - y_k)). \tag{12}$$

The covariance is updated as follows:

$$\boldsymbol{P}_{k|k} = \boldsymbol{P}_{k|k-1} + \boldsymbol{K}\boldsymbol{P}_{yy}\boldsymbol{K}^T. \tag{13}$$

3.3.4 Estimation of tip position

The control input to the UKF presented above is $\boldsymbol{p}^{tip}_r$, which is the position of the tip of the robot in the frame of the base of the robot. At every iteration of the UKF, $\boldsymbol{p}^{tip}_r$ is estimated using another UKF. The state vector of this second UKF is $\boldsymbol{q}_k = \boldsymbol{p}^{tip}_r \in \mathbb{R}^3$. The process model for the filter uses a constant velocity motion model:

$$\boldsymbol{q}_{k|k-1} = \boldsymbol{q}_{k-1|k-1} + \boldsymbol{v}\Delta t,$$
$$\boldsymbol{Q}_{k|k-1} = \boldsymbol{Q}_{k-1|k-1} + \boldsymbol{N},$$

where $\boldsymbol{v} = (\boldsymbol{q}_{k-1|k-1} - \boldsymbol{q}_{k-2|k-2})/\Delta t$ and Δt is the time elapsed between two successive filtering loops and N is the uncertainty in the process model that helps take care of unmodelled scenarios such as change of direction of motion, accuracy of the robot etc. The measurement model for this filter is:

$$\boldsymbol{h}(\boldsymbol{q}) = \boldsymbol{q},$$

The sensor measurement is the tip position: $\boldsymbol{z}_k = \boldsymbol{p}^s$. The sigma points and weights are computed using Eq. 5 and Eq. 10 respectively, with the dimensionality of the state vector $M = 3$. Since the

4 EXPERIMENTAL SETUP

To demonstrate the validity of the proposed approach, palpation experiments at various constant forces were carried out, as outlined in Section 3.1. The experimental setup consisted of a 3-DOF cartesian robot equipped with a force/torque sensor (ATI Gamma F/T Transducer, S/N: FT8578) with an attached spherical probe 12.7 mm in diameter (see Fig 4. Centralized computed torque control for the Cartesian robot was implemented in a real-time system running at 1 kHz. Hybrid-force control was used for raster positioning a silicone tissue phantom (M-F Manufacturing), wherein force control was applied in along the local surface normal computed from the F/T sensor, and position control was applied along the orthogonal direction. Further details on the control architecture can be found in [8].

Five consecutive force-controlled scans were carried out from 1.0 N to 3.0 N at intervals of 0.5 N. We observed that at higher forces, there was considerable distortion in the phantom tissue, due to which data acquired at these forces were not considered in the registration process.

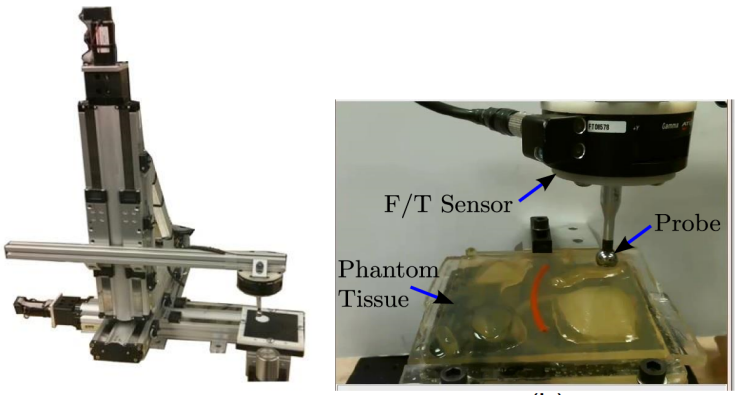

Figure 4: (a) 3-DOF Cartesian Robot and (b) Experimental setup with the probe palpating the phantom tissue.

5 RESULTS

As a first step, the ground truth stiffness maps were computed for various forces as described in Section 3.1. The stiffness maps for three sample forces are shown in Fig. 2. Since the stiffness computations are interpolated over the surface of the organ by using a grid mesh of points taken along a plane and projected to the surface, the estimates are poor at the regions where the surface

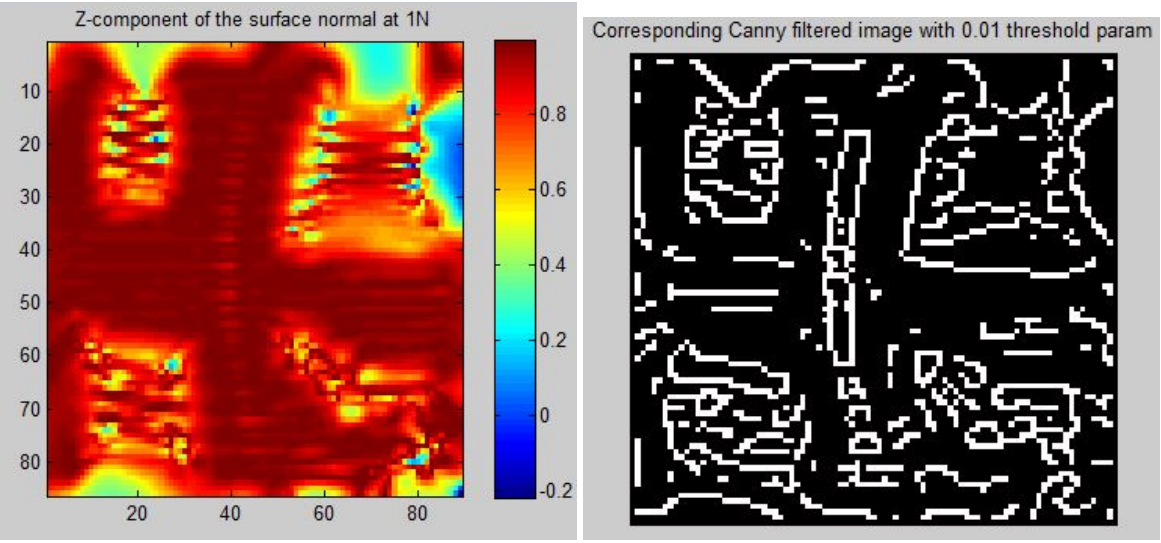

(a) Contour plot of the variation in surface normal over the surface of the model

(b) The white regions show high variation in surface normal orientation

Figure 5: Plots showing variation in surface normal across the surface of the organ and the regions with high variation in surface normal orientation.

The location of the organ with respect to the base of the robot was carefully measured to provide a ground truth registration, in order to measure how good our estimated registration is. The ground truth registration is:

$$\boldsymbol{T} = \begin{pmatrix} 0.9996 & 0.0276 & 0.0101 & -34.7452 \\ -0.0278 & 0.9995 & 0.0171 & -7.2757 \\ -0.0096 & -0.0174 & 0.9998 & 16.3866 \\ 0 & 0 & 0 & 1.0000 \end{pmatrix}. \tag{14}$$

The surface is first palpated at two force levels, 1N and 1.5N at arbitrary locations. The tip location is sensed in both these experiments and a stiffness map is generated from this data following the approach shown in Section 3.1. The stiffness map generated is as shown in Fig. 3. Upon performing a pre-registration as shown in Section 3.2 we obtain the following transformation matrix:

$$\boldsymbol{T} = \begin{pmatrix} 0.9990 & 0.0436 & 0.0104 & -34.8915 \\ -0.0438 & 0.9989 & 0.0169 & -6.5140 \\ -0.0096 & -0.0174 & 0.9998 & 16.3866 \\ 0 & 0 & 0 & 1.0000 \end{pmatrix}. \tag{15}$$

Having performed the pre registration, the surface was raster scanned as shown in Fig. 6 with a

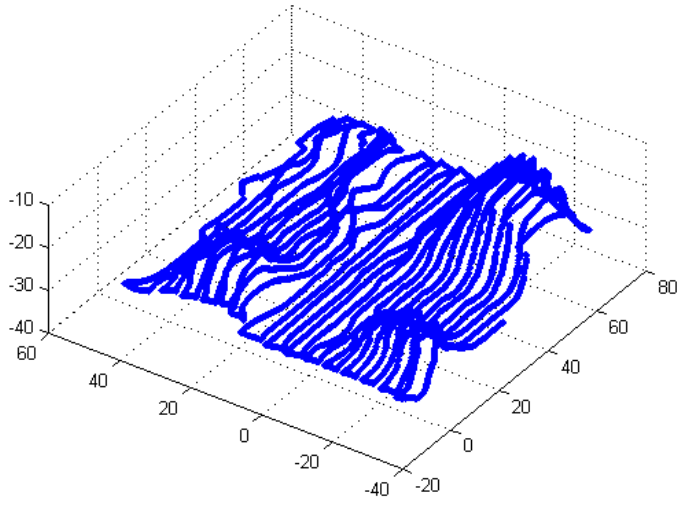

Figure 6: Raster path that was used to palpate the silicon model

to the surface of the model as shown in Fig. 7. The final registration as estimated by the filter was:

$$\boldsymbol{T} = \begin{pmatrix} 0.9989 & -0.0316 & 0.0333 & -34.5227 \\ 0.0320 & 0.9994 & -0.0111 & -8.5058 \\ -0.0329 & 0.0122 & 0.9994 & 16.7827 \\ 0 & 0 & 0 & 1.0000 \end{pmatrix},$$

which is very close to the ground truth. When the registration estimation was performed without using the palpation trajectory model, the estimates for tip position took longer time to converge.

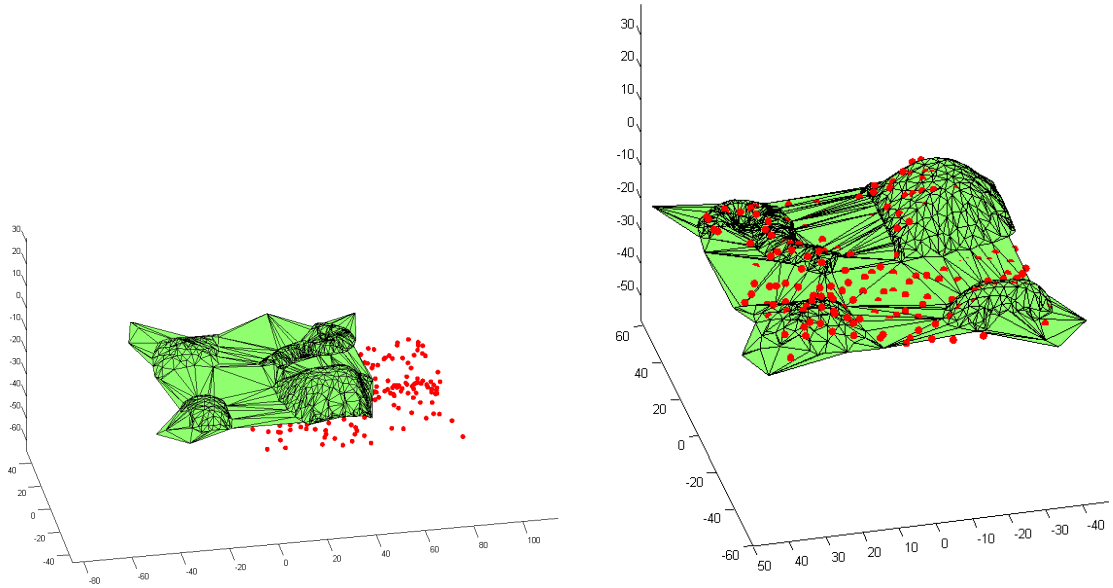

(a) The red dots represent the palpation points in the

(b) The red dots represent the palpation points in the

A sample result for a failed registration is as shown in Fig. 8. This example demonstrates the importance of the pre-registration step. The registration was also estimated using an iterative extended Kalman filter (IEKF) instead of UKF and the results obtained were found to be very similar.

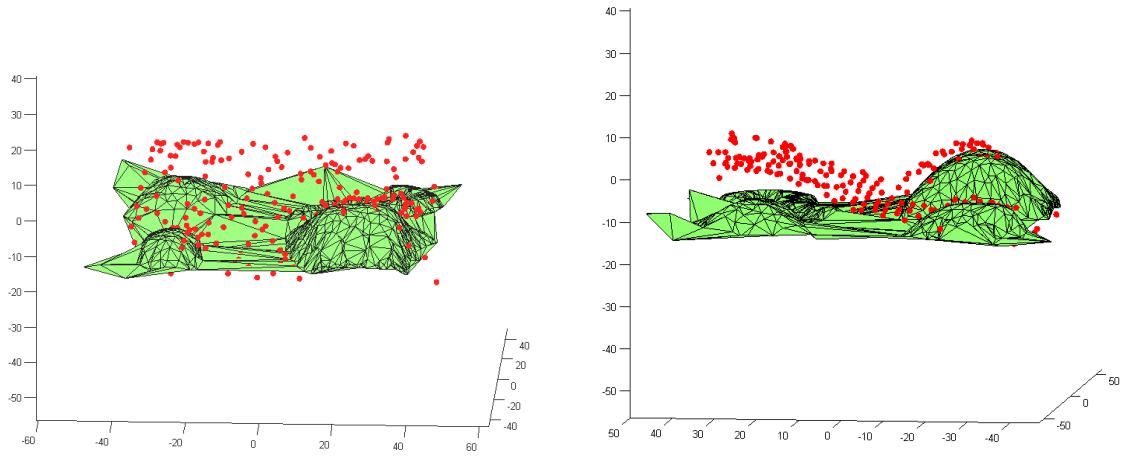

(a) The red dots represent the palpation points in the frame of the organ model before registration

(b) The red dots represent the palpation points in the frame of the organ model after registration

Figure 8: Example of bad registration when the intial guess for UKF is not chosen from the pre registration step.

6 CONCLUSIONS

This paper outlines a probabilistic approach based on unscented Kalman filtering to register a deformable object to a surgical tool using mechanical stiffness information obtained by palpating the object. We assumed a realistic deformation dependent stiffness model obtained by raster-scanning the object at varying forces along the local surface normal of the object using a 3-DOF Cartesian robot. Subsequently, the stiffness distribution at a given scan force was used to pre-register the object to the robot tip. In addition, a pre-defined palpation trajectory was used to specify the process model of the filtering algorithm instead of uniformative distribution of the palpation path.

To the best of the authors' knowledge, this paper presents for the first time, a mechanical palpation based pre-registration step to provide a good initial guess to the registration process. One of the key findings of this paper is that a pre-registration step significantly improves registration

In this work, we did not consider global deformations in the deformation during palpation. This is not an unlikely scenario, since anatomical structures are typically geometrically unconstrained and could move globally during the palpation process. In the future, we will focus on accounting for global deformations in the registration process.

References

[1] K.S. Arun, T.S Huang, and S.D. Bolstein. Least-Squares Fitting of Two 3-D Point Sets. *IEEE Transactions on Pattern Analysis and Machine Intelligence*, 9(5):698–700, 1987.

[2] P. Besl. A Method for Registration of 3-D Shapes. *IEEE Transactions on Pattern Analysis and Machine Intelligence*, 14(2):239–256, 1992.

[3] P.J. Besl and Neil D. McKay. A method for registration of 3-d shapes. *Pattern Analysis and Machine Intelligence, IEEE Transactions on*, 14(2):239–256, Feb 1992.

[4] Amir Degani, Howie Choset, Alon Wolf, and Marco A Zenati. Highly articulated robotic probe for minimally invasive surgery. In *Robotics and Automation, 2006. ICRA 2006. Proceedings 2006 IEEE International Conference on*, pages 4167–4172. IEEE, 2006.

[5] V. Egorov and A.P. Sarvazyan. Mechanical Imaging of the Breast. *IEEE Transactions on Medical Imaging*, 27(9):1275–1287, 2008.

[6] Y.C. Fung. *Biomechanics: Mechanical Properties of Living Tissues*. Springer, second edition, 1993.

[7] Matthew Gettman and Jeffrey Cadeddu. Natural Orifice Translumenal Endoscopic surgery (NOTES) in Urology: Initial Experience. *Journal of Endourology*, 22(4):783–788, 2008.

[8] R. Goldman, A. Bajo, and N. Simaan. Algorithms for autonomous exploration and estimation in compliant environments. *Robotica*, 31(1):71–87, 2013.

[9] Søren Hauberg, François Lauze, and Kim S. Pedersen. Unscented Kalman Filtering on Riemannian Manifolds. *Journal of Mathematical Imaging and Vision*, pages 1–18, August 2012.

[10] B. Horn. Closed-form solution of absolute orientation using unit quaternions. *Journal of the Optical Society of America A*, 4:629–642, 1987.

[12] Andrew Long, Kevin Wolfe, Michael Mashner, and Gregory Chirikjian. The Banana Distribution is Gaussian: A Localization Study with Exponential Coordinates. In *Proceedings of Robotics: Science and Systems*, Sydney, Australia, July 2012.

[13] A.S. Naini, R.V. Patel, and A. Samani. Measurement of Lung Hyperelastic Properties Using Iinverse Finite Element Approach. *IEEE Transactions on Biomedical Engineering*, 58(10):2852–2859, 2011.

[14] Arun Rangaprasad, Matthew Travers, and Howie Choset. Using lie algebra to estimate the shape of medical snake robots. In *Proceedings of the 27th IEEE/RSJ International Conference on Intelligent Robots and Systems (IROS)*, September 2014.

[15] R. Sagawa, K. Akasaka, Y. Yagi, and L. Van Gool. Elastic convolved ICP for the registration of deformable objects. In *IEEE 12th International Conference on Computer Vision Workshop*, pages 1558–1565, 2009.

[16] Siddharth Sanan, Stephen Tully, Andrea Bajo, Nabil Simaan, and Howie Choset. Simultaneous compliance and registration estimation for robotic surgery. In *Proceedings of the Robotics: Science and Systems Conference*, 2014.

[17] K. Sangpradit, H. Liu, L. Seneviratne, and K. Althoefer. Tissue Identification using Inverse Finite Element Analysis of Rolling Indentation. In *In IEEE International Conference on Robotics and Automation*, pages 1250–1255, 2009.

[18] J. M. Selig. *Geometric fundamentals of robotics*. Springer, New York, second edition, 1996.

[19] Nabil Simaan, Russell Taylor, and Paul Flint. A dexterous system for laryngeal surgery. In *Robotics and Automation, 2004. Proceedings. ICRA'04. 2004 IEEE International Conference on*, volume 1, pages 351–357. IEEE, 2004.

[20] A. Sotiras, C. Davatzikos, and N. Paragios. Deformable Medical Image Registration: A Survey. *IEEE Transactions on Medical Imaging*, 32(7):1153–1190, 2013.

[21] Stephen Tully, George Kantor, and Howie Choset. Inequality constrained kalman filtering for the localization and registration of a surgical robot. In *Intelligent Robots and Systems (IROS), 2011 IEEE/RSJ International Conference on*, pages 5147–5152. IEEE, 2011.

[22] E.A Wan and R. Van der Merwe. The unscented kalman filter for nonlinear estimation. In *Adaptive Systems for Signal Processing, Communications, and Control Symposium 2000. AS-SPCC. The IEEE 2000*, pages 153–158, 2000.

[23] P.S. Wellman, E.P. Dalton, D. Krag, K.A. Kern, and R.D. Howe. Tactile imaging of breast masses: first clinical report. *Archives of Surgery*, 136(2):204–208, 2001.

[24] Tomonori Yamamoto, Michael Bernhardt, Angelika Peer, Martin Buss, and Allison M. Okamura. Techniques for Environment Parameter Estimation During Telemanipulation. In *Proceedings of the 2nd Biennial IEEE/RAS-EMBS International Conference on Biomedical Robotics and Biomechatronics*, pages 217–223, 2008.